

Linear spectropolarimetry of polarimetric standard stars with VLT/FORS2[★]

Aleksandar Cikota^{1†}, Ferdinando Patat¹, Stefan Cikota², Tamar Faran¹

¹European Southern Observatory, Karl-Schwarzschild-Str. 2, 85748 Garching b. München, Germany

²Physics Department, University of Split, Ruđera Boškovića 33, 21000 Split, Croatia

Accepted XXX. Received YYY; in original form ZZZ

ABSTRACT

We reduced ESO’s archival linear spectropolarimetry data (4000–9000Å) of 6 highly polarized and 8 unpolarized standard stars observed between 2010 and 2016, for a total of 70 epochs, with the FOcal Reducer and low dispersion Spectrograph (FORS2) mounted at the Very Large Telescope. We provide very accurate standard stars polarization measurements as a function of wavelength, and test the performance of the spectropolarimetric mode (PMOS) of FORS2. We used the unpolarized stars to test the time stability of the PMOS mode, and found a small ($\leq 0.1\%$), but statistically significant, on-axis instrumental polarization wavelength dependency, possibly caused by the tilted surfaces of the dispersive element. The polarization degree and angle are found to be stable at the level of $\leq 0.1\%$ and ≤ 0.2 degrees, respectively. We derived the polarization wavelength dependence of the polarized standard stars and found that, in general, the results are consistent with those reported in the literature, e.g. [Fossati et al. \(2007\)](#) who performed a similar analysis using FORS1 data. The re-calibrated data provide a very accurate set of standards that can be very reliably used for technical and scientific purposes. The analysis of the Serkowski parameters revealed a systematic deviation from the width parameter K reported by [Whittet et al. \(1992\)](#). This is most likely explained by incorrect effective wavelengths adopted in that study for the R and I bands.

Key words: stars: general – instrumentation: polarimeters – (ISM:) dust, extinction

1 INTRODUCTION

Spectropolarimetry is a technique that provides additional information to those given by simple intensity measurements. For instance, linear spectropolarimetry can probe the geometry of Supernova explosions (see [Wang & Wheeler \(2008\)](#) for a comprehensive review), circumstellar and interstellar dust properties (see e.g. [Serkowski et al. \(1975\)](#)), and the magnetic fields of galaxies (see e.g. [Scarrott \(1996\)](#), [Scarrott et al. \(1996\)](#)).

Given the comparatively low levels of polarization that are typical in this kind of studies, it is important the polarimeter being used is properly calibrated. The main aim of this work is to provide a re-calibration of a sub-set of highly polarized standard stars, which are not too bright to be observed with large telescopes, and can be used to verify the performance of other similar instruments in the

southern hemisphere. In addition, related to the fact that ESO’s Quality Control Group monitors polarimetric standards since 2009, we test the performance of the FOcal Reducer and low dispersion Spectrograph (FORS2) instrument mounted at the Very Large Telescope (VLT), in terms of stability and accuracy, by means of a thorough analysis of archival calibration data of highly linearly polarized and unpolarized standard stars.

[Fossati et al. \(2007\)](#) presented an analysis of standard stars observations obtained between 1999 and 2005 in PMOS and imaging-polarimetry (IPOL) mode with FORS1. They investigated the FORS1 stability in both, PMOS and IPOL mode, and found a small instrumental offset in the Stokes Q parameter which appears in PMOS mode only. This study is meant to further investigate and characterize that offset using FORS2 data.

[★] Based on archival calibration data collected at the European Organisation for Astronomical Research in the Southern Hemisphere.

[†] E-mail: acikota@eso.org

2 INSTRUMENTAL SETUP AND OBSERVATIONS

FORS2 is currently mounted at the Cassegrain focus of the ESO's Antu VLT unit. This focal reducer is equipped with a polarimetric mode, which can be selected by introducing in the light path a Wollaston prism and a rotatable super-achromatic half-wave retarder plate coupled to a grism and/or a filter to perform linear imaging or spectro-polarimetry (Appenzeller 1967; Appenzeller et al. 1998; ESO 2015).

For our purposes, we selected eight standard stars with zero polarization, and six highly polarized standard stars extracted from the FORS Standard Fields and Stars list¹ (listed in Table 1). All stars from the FORS Standard Fields and Stars list (i.e. our sample), were also analyzed by Fossati et al. (2007). They additionally considered three polarized standard stars (HD 345310, HD 111579 and BD -13 5073), 8 unpolarized stars (WD 2359-434, WD 0310-688, WD 1616-154, WD 1620-391, HD 176425, WD 2007-303, WD 2039-202, WD 2149+021) and HD 64299, which was erroneously suggested as an unpolarized standard star, but is in fact polarized at the 0.1% level (see e.g. Masiero et al. (2007)).

From the archive we selected observations obtained in PMOS mode with grism 300V, without an order separating filter, and with the half-wave retarder plate positioned at angles of 0°, 22.5°, 45°, and 67.5°. The half-wave retarder plate angle is measured between the acceptance axis of the ordinary beam of the Wollaston prism (which is aligned to the north-south direction) and the fast axis of the retarder plate. In order to allow a time trend analysis, the stars were selected to have observations at multiple epochs (40 epochs in total of unpolarized, and 30 of polarized stars), spanning 5 years. The stars were placed on the central slit of the PMOS focal mask, very close to the optical axis of the instrument. The spectrum produced by the grism is split by the Wollaston prism into an ordinary (o) and extraordinary (e) beam, which are separated by a throw of about 22 arcseconds.

3 DATA REDUCTION

After excluding saturated frames, the data were reduced using standard procedures in IRAF. Wavelength calibration was achieved using He-Ne-Ar arc lamp exposure. The typical RMS accuracy is $\sim 0.3 \text{ \AA}$. Although it is very difficult to achieve a complete flat fielding correction in the presence of polarization optics, the effects of improper correction were minimized by taking advantage of the redundant number of half-wave positions (see Patat & Romaniello (2006)).

Ordinary and extra-ordinary beams were extracted in an unsupervised way using the PyRAF `apextract.apall` procedure, with a fixed aperture size of 10 pixels. To avoid spectrum tracing problems, the input frames were properly trimmed to exclude the low signal-to-noise at the edges of the spectral range. The final effective wavelength range is 3950-9300 \AA . We calculated the total flux in *BVRI* passbands by integrating the total flux weighted with Bessel's

BVRI passband filters, and computed the synthetic broadband polarization degree and polarization angle corresponding to each passband. We also binned the spectra in 50 \AA bins, in order to obtain a larger signal-to-noise ratio, and calculated the Stokes parameters Q and U , polarization degree P , and polarization angle θ_P as a function of wavelength. The signal-to-noise ratio (SNR) is typically between 500 and 2000 per 50 \AA bin, tabulated for each individual epoch at a given wavelength in Table 4 and Table 5 for unpolarized and polarized standard stars respectively.

The Stokes parameters Q and U were derived via Fourier transformation, as described in the FORS2 User Manual:

$$\begin{aligned} Q &= \frac{2}{N} \sum_{i=0}^{N-1} F(\theta_i) \cos(4\theta_i) \\ U &= \frac{2}{N} \sum_{i=0}^{N-1} F(\theta_i) \sin(4\theta_i) \end{aligned} \quad (1)$$

where $F(\theta_i)$ are the normalized flux differences between the ordinary (f^o) and extra-ordinary (f^e) beams:

$$F(\theta_i) = \frac{f^o(\theta_i) - f^e(\theta_i)}{f^o(\theta_i) + f^e(\theta_i)} \quad (2)$$

at different half-wave retarder plate position angles $\theta_i = i * 22.5^\circ$.

Although FORS2 is equipped with a super-achromatic half wave plate, residual retardance chromatism is present. The wavelength dependent retardance offset ($-\Delta\theta(\lambda)$) is tabulated in the FORS2 User Manual (ESO 2015). The chromatism was corrected through the following rotation of the Stokes parameters (Bagnulo et al. 2009; Patat & Taubenberger 2011):

$$\begin{aligned} Q_{\text{corrected}} &= Q \cos 2\Delta\theta(\lambda) - U \sin 2\Delta\theta(\lambda) \\ U_{\text{corrected}} &= Q \sin 2\Delta\theta(\lambda) + U \cos 2\Delta\theta(\lambda) \end{aligned} \quad (3)$$

Hereafter, $Q_{\text{corrected}}$ and $U_{\text{corrected}}$ are noted as Q and U .

Finally we calculate the polarization (eq. 4):

$$P = \sqrt{Q^2 + U^2} \quad (4)$$

and the polarization angle (eq. 5),

$$\theta = \frac{1}{2} \arctan(U/Q). \quad (5)$$

The statistical uncertainties were estimated using the prescriptions presented by Patat & Romaniello (2006).

The classical Serkowski parameters (Serkowski et al. (1975), eq. 6) were finally derived by linear least squares fits to the linear polarization $P(\lambda)$, yielding the peak polarization level (P_{max}) and wavelength (λ_{max}), and the width constant (K).

$$\frac{P(\lambda)}{P_{\text{max}}} = \exp \left[-K \ln^2 \left(\frac{\lambda_{\text{max}}}{\lambda} \right) \right] \quad (6)$$

4 RESULTS AND DISCUSSION

4.1 Unpolarized stars

The analysis of FORS2 linear polarization stability and accuracy is based on eight unpolarized standard stars, observed at 40 epochs in total, between 2010 and 2015 (see Table 1). For all stars and each epoch, we calculated the mean value of the Stokes parameters P_Q and P_U in the 3950-9300 \AA wavelength range (Passband "all" in Table 4), which is shown in Figure 1. The values do not show statistically

¹ https://www.eso.org/sci/facilities/paranal/instruments/fors/tools/FORS_Std.html

Table 1. List of observed standard stars.

Name	RA (J2000)	DEC (J2000)	V (mag)	Spec. type	Type	No. of Epochs
HD 10038	01 37 18.59	-40 10 38.46	8.1	A2mA5-F0	unPol.	8
HD 13588	02 11 16.69	-46 35 06.17	7.9	A1m	unPol.	4
HD 42078	06 06 41.04	-42 17 55.69	6.2	Am	unPol.	5
HD 97689	11 13 50.75	-52 51 21.22	6.8	A0m	unPol.	12
WD 1615-154	16 17 55.26	-15 35 51.93	13.4	DA1.7	unPol.	1
WD 1620-391	16 23 33.84	-39 13 46.16	11.0	DA2	unPol.	7
WD 2039-202	20 42 34.75	-20 04 35.95	12.4	DA2.5	unPol.	2
WD 2149+021	21 52 25.38	+02 23 19.54	12.7	DA2.8	unPol.	1
NGC 2024 1	05 41 37.85	-01 54 36.5	12.2	B0.5V	Pol.	7
Vela1 95 ^a	09 06 00.01	-47 18 58.2	12.1	OB+	Pol.	11
Hiltner 652 ^b	17 43 19.59	-28 40 32.76	10.8	B1II-III	Pol.	8
HDE 316232	17 45 43.70	-29 13 18.15	10.4	O9IV	Pol.	1
BD -14 4922	18 11 58.10	-14 56 09.01	9.73	O9.5	Pol.	2
BD -12 5133	18 40 01.70	-12 24 06.92	10.4	B1V	Pol.	1

The coordinates, brightness and spectral type were taken from the SIMBAD Astronomical Database. Type indicates if the star is polarized (Pol.) or unpolarized (unPol.), and No. of Epochs is the number of epochs.

^a in Fossati et al. (2007) designated as Ve 6-23.

^b in Fossati et al. (2007) designated as CD-28 13479.

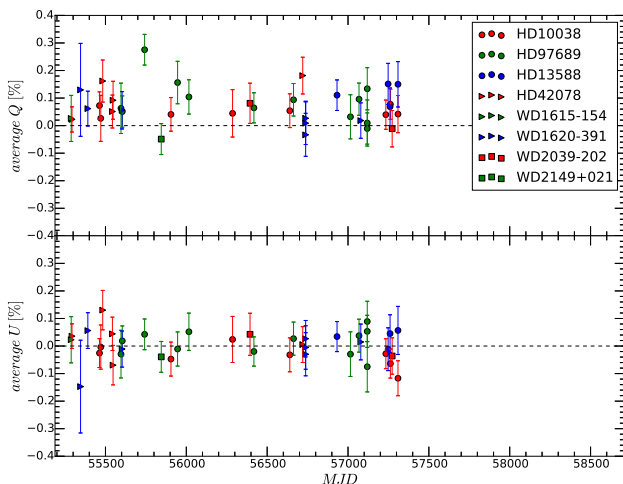


Figure 1. Averaged Stokes parameters P_Q and P_U for the 8 unpolarized standard stars in the sample observed on 40 different epochs.

significant variations over the full time range, with very similar standard deviations of P_Q and P_U . However, a small but statistically significant instrumental offset is detected in P_Q . The weighted mean of the Stokes parameter P_Q of all stars and epochs is $0.07 \pm 0.01\%$, while the corresponding value for P_U is $0.00 \pm 0.01\%$.

To investigate possible wavelength dependent effects, we calculated the weighted mean of P_Q and P_U as a function of wavelength using all observations of unpolarized standard stars. A clear, wavelength dependent offset is detected in Q (Figure 2). The first-order, best fit laws (red lines in Figure 2) are as follows:

$$Q(\lambda) = [(9.66 \pm 1.04) \times 10^{-8}] \lambda + (3.29 \pm 6.34) \times 10^{-5} \quad (7)$$

$$U(\lambda) = [(7.28 \pm 0.90) \times 10^{-8}] \lambda - (4.54 \pm 0.55) \times 10^{-4}$$

where λ is expressed in \AA . These relations provide a handy correction to be applied to the observed Q and U values. Rigorously speaking, this implicitly assumes that the correction is additive and does not depend on the incoming signal. This approximation probably holds only to first order. The exact prescription can only be obtained with a proper characterization of the Mueller matrices that describe the optical system, which is beyond the scope of this paper.

Fossati et al. (2007) performed a similar analysis using observations of standard stars obtained with FORS1 from 1999 to 2005 in both spectropolarimetric (PMOS) and imaging polarimetry (IPOL) mode. For PMOS, they found that the weighted average of all P_U values in PMOS mode are consistent with a null value, but detected an offset of $0.07 \pm 0.01\%$, and $0.09 \pm 0.01\%$ in $P_Q(B)$ and $P_Q(V)$ respectively. They did not detect any offset in IPOL mode, and concluded that the P_Q offset may be associated with some, but not all, grism and filter combinations.

Our results, based on observations that were taken through the 300V grism (ID: +10) and no order-sorting filters, confirm the findings of Fossati et al. (2007) and lead us to conclude that the source of the instrumental polarization causing the offset in P_Q probably resides in the inclined surface of the prism that is coupled to the transmission grating in the FORS1 and FORS2 grisms.

4.2 Polarized stars

For our analysis we reduced a sample of six highly polarized standard stars (Table 1) observed with FORS2 between 2009 and 2015 on 30 different epochs. The data were corrected for instrumental polarization using the relations derived from

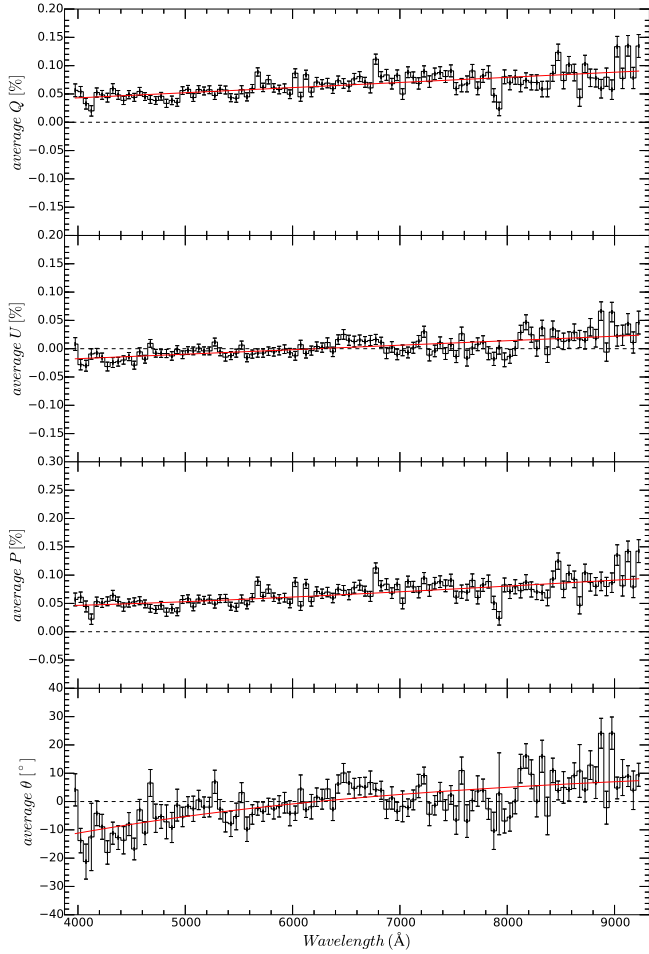


Figure 2. Weighted means of Stokes parameters Q and U of all observations of unpolarized stars (8 objects, 40 epochs). The red lines are linear least-squares fits to the weighted averages Q and U . The polarization P and polarization angle θ were calculated from the weighted means of Q and U . The red curves over-plotted on P and θ were calculated from separate linear fits to $Q(\lambda)$ and $U(\lambda)$.

the unpolarised stars (Eqs. 7). The results for the individual epochs are given in Table 5, while weighted means of all epochs are listed in Table 2. An example of polarization wavelength dependence is shown in Figure 3, and a Q/U diagram in Figure 4. As expected for polarization generated by interstellar dust sharing the same alignment angle, the polarization angle is constant, and the points on the Q/U diagram follow a straight line.

The wavelength dependence of the polarization angle was characterized by fitting a second order polynomial to the calculated weighted mean of the polarization angle (Figure 5). From the values of the best fit coefficients we conclude that there is no significant $\theta - \lambda$ dependence. The polarization angles are all constant to within the measurement errors, with slopes $d\theta/d\lambda$ between -2.5 and 0.53 degree/ μm .

We tested the reproducibility of the observations using stars observed at least at two epochs: Vela1 95, Hiltner 652, NGC 2024 1 and BD-144922. An example for Vela1 95 is presented in Fig. 6. The root mean square deviation from the mean polarization values are 0.21% (Vela1 95, 11

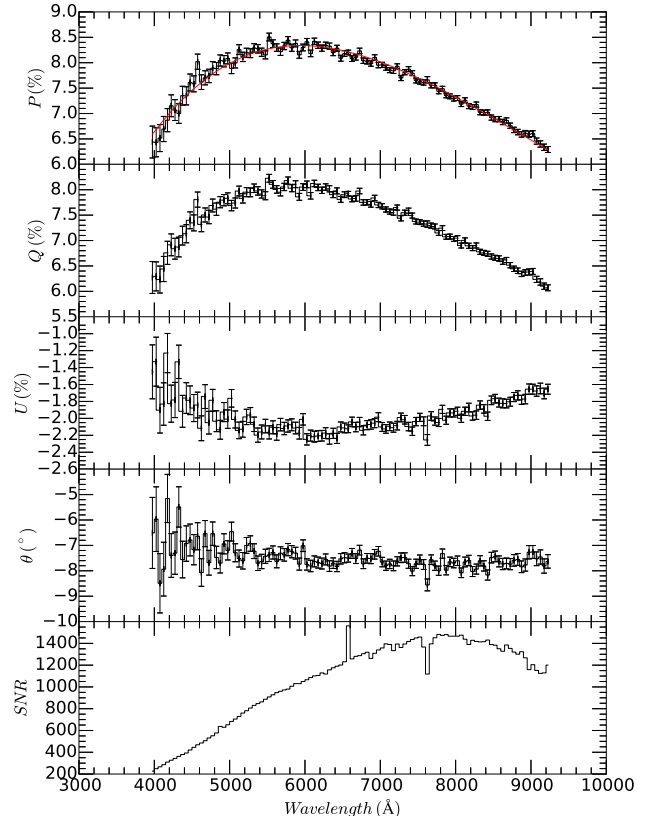


Figure 3. Total polarization P , Stokes parameters Q and U , Polarization angle θ and SNR for Vela1 95 at epoch 2014-01-06. The bin width is 50 \AA . The solid red line is the best fit Serkowski law.

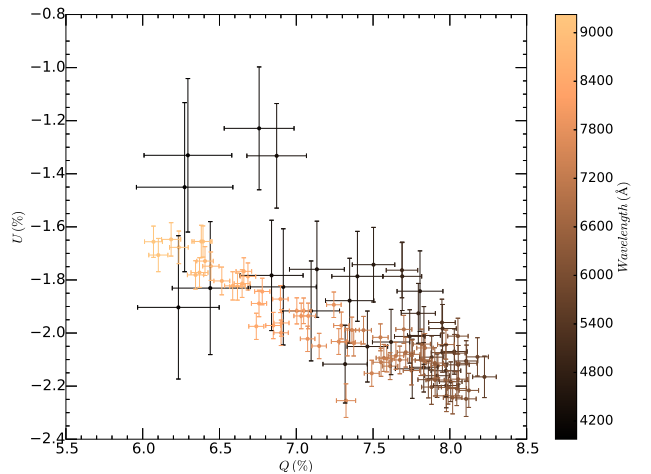


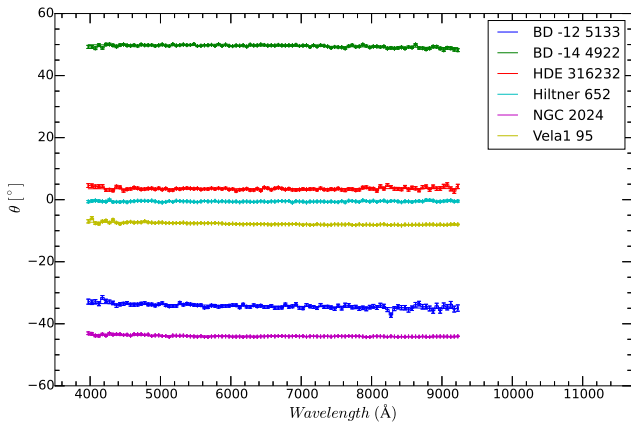
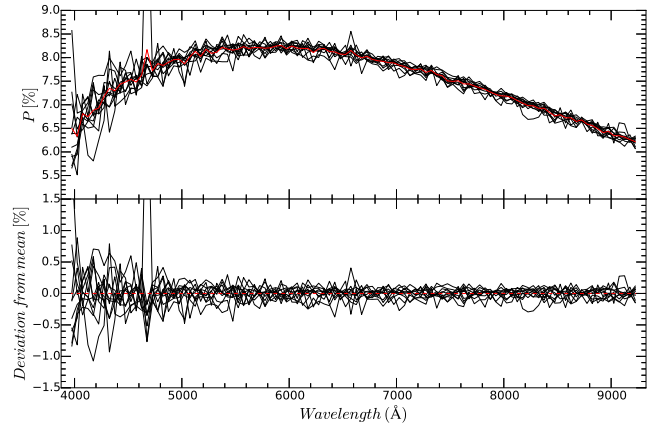
Figure 4. Q/U diagram for Vela1 95 at epoch 2014-01-06. The wavelength is color coded.

epochs), 0.12% (Hiltner 652, 8 epochs), 0.12% (NGC 2024 1, 7 epochs), and 0.05% (BD-144922, 2 epochs).

We finally tested the HWP positioning stability, by calculating the residuals of the mean $\theta(\lambda)$ values for all epochs of the polarized stars. No systematic jumps are detected, while erratic fluctuations are present, with a peak-to-peak amplitude of about 1.2° and a standard deviation of 0.27°

Table 2. Weighted averages of polarized standard stars observed with FORS2.

Name	Passband	P (%)	P_Q (%)	P_U (%)	θ ($^\circ$)	Serkowski law		
						λ_{\max} (\AA)	P_{\max} (%)	K
Vela1 95		7.645 ± 0.044	7.445 ± 0.044	-1.739 ± 0.046	172.76 ± 0.05	5864.5 ± 7.4	8.295 ± 0.004	1.34 ± 0.01
	B	7.645 ± 0.044	7.445 ± 0.044	-1.739 ± 0.046	172.76 ± 0.05			
	V	8.163 ± 0.011	7.834 ± 0.011	-2.295 ± 0.012	172.41 ± 0.02			
	R	7.927 ± 0.003	7.56 ± 0.003	-2.383 ± 0.003	172.06 ± 0.01			
BD -14 4922	I	7.151 ± 0.002	6.9 ± 0.002	-1.881 ± 0.002	171.95 ± 0.01	5452.5 ± 13.9	6.137 ± 0.007	1.3 ± 0.02
	B	5.801 ± 0.024	-0.992 ± 0.024	5.715 ± 0.024	49.7 ± 0.07			
	V	6.096 ± 0.012	-0.955 ± 0.012	6.021 ± 0.012	49.8 ± 0.05			
	R	5.818 ± 0.006	-0.864 ± 0.005	5.753 ± 0.006	49.7 ± 0.04			
HDE 316232	I	4.99 ± 0.006	-0.796 ± 0.006	4.926 ± 0.006	49.24 ± 0.05	5591.1 ± 18.3	5.017 ± 0.008	1.2 ± 0.03
	B	4.679 ± 0.023	4.637 ± 0.023	0.619 ± 0.021	3.61 ± 0.09			
	V	4.931 ± 0.014	4.901 ± 0.014	0.547 ± 0.012	3.51 ± 0.07			
	R	4.772 ± 0.007	4.745 ± 0.007	0.508 ± 0.006	3.37 ± 0.06			
Hiltner 652	I	4.214 ± 0.008	4.176 ± 0.008	0.562 ± 0.007	3.53 ± 0.08	5776.5 ± 9.0	6.467 ± 0.005	1.17 ± 0.01
	B	5.948 ± 0.017	5.948 ± 0.017	-0.054 ± 0.017	179.52 ± 0.05			
	V	6.371 ± 0.009	6.367 ± 0.009	-0.198 ± 0.009	179.44 ± 0.03			
	R	6.218 ± 0.004	6.214 ± 0.004	-0.218 ± 0.004	179.39 ± 0.03			
NGC 2024 1	I	5.613 ± 0.004	5.612 ± 0.004	-0.041 ± 0.004	179.46 ± 0.03	6340.4 ± 4.7	9.855 ± 0.004	1.29 ± 0.01
	B	8.602 ± 0.044	0.583 ± 0.045	-8.582 ± 0.044	136.43 ± 0.05			
	V	9.548 ± 0.013	0.122 ± 0.013	-9.546 ± 0.013	135.94 ± 0.02			
	R	9.671 ± 0.004	-0.0 ± 0.004	-9.67 ± 0.004	135.93 ± 0.01			
BD -12 5133	I	9.009 ± 0.002	0.398 ± 0.002	-8.999 ± 0.002	135.9 ± 0.01	5049.5 ± 35.5	4.369 ± 0.01	1.2 ± 0.04
	B	4.217 ± 0.027	1.688 ± 0.027	-3.865 ± 0.027	146.54 ± 0.12			
	V	4.266 ± 0.016	1.568 ± 0.016	-3.968 ± 0.016	145.88 ± 0.09			
	R	3.996 ± 0.008	1.406 ± 0.008	-3.74 ± 0.008	145.62 ± 0.08			
	I	3.348 ± 0.009	1.222 ± 0.009	-3.117 ± 0.009	145.28 ± 0.11			

**Figure 5.** Weighted mean of polarization angle θ as a function of wavelength.**Figure 6.** Reproducibility of Vela1 95 polarization P . The bin width is 50 \AA . The solid red line is the mean polarization of all 11 epochs. The deviations from the mean are shown in the bottom plot. The RMS of the deviation from the mean value is 0.21%.

(Figure 7). Given the typical statistical errors of the single measurements, the observed fluctuations are statistically very significant and certainly not due to the photon noise. The most likely interpretation is a possible drift in the absolute positioning of the retarder plate and/or of the analyzer. The estimated rms deviation (~ 0.3 degrees) hence represents the typical maximum accuracy one can expect on the polarization angle for very high signal-to-noise ratios.

4.2.1 Comparison with the literature

We compared our synthetic broad-band results (Table 2) to those reported by Fossati et al. (2007) (their Table 2) and the values based on data taken with FORS1 during commis-

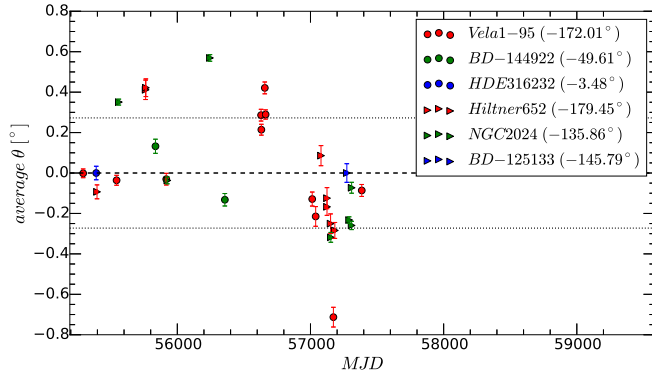


Figure 7. Polarization angle stability. Shown are residuals of the averaged $\theta(\lambda)$ values for 30 epochs of 6 polarized standard stars.

sioning, given in the FORS webpage². Figure 8 shows the polarization and polarization angle differences, ΔP and $\Delta\theta$, between our measurements and those published in the literature: $\Delta P = P_{\text{Literature}} - P_{\text{This work}}$ and $\Delta\theta = \theta_{\text{Literature}} - \theta_{\text{This work}}$.

The average polarization deviation of all values, $\langle\Delta P\rangle$, obtained in PMOS mode by Fossati et al. (2007) from values obtained in this work is 0.01%, with a root mean square deviation of 0.17%. Also the values obtained by Fossati et al. (2007) in IPOL mode are consistent with our results, with an average $\langle\Delta P\rangle$ of -0.02% and an RMS of 0.15%. Our results are on average larger than the values given in the FORS webpage, with $\langle\Delta P\rangle = -0.15\%$ and an RMS of 0.36%.

For the polarization angle, the average deviation from the PMOS values given in Fossati et al. (2007) is $\langle\Delta\theta\rangle=0.17^\circ$, with an RMS of 0.91° ; $\langle\Delta\theta\rangle=-0.03^\circ$, with an RMS of 0.77° for IPOL mode values (Fossati et al. 2007); and $\langle\Delta\theta\rangle=0.50^\circ$, with an RMS of 0.76° for the values given in the FORS webpage.

Thus, our results are, in general, in good agreement with previous estimates. The discrepancies with results given in Fossati et al. (2007) are consistent with the RMS variation found in the repeatability test (RMS $\leq 0.2\%$, see § 4.2), and might be due to star variability or instrumental effects (e.g. the HWP positioning uncertainty, see Figure 7), while the discrepancy from the values given in the FORS webpage is probably due to systematic differences between FORS2 and FORS1.

We also compared our Serkowski law fitting results for the 6 polarized standard stars to a data set of 105 objects studied by Whittet et al. (1992). They collected data obtained polarimetric observation in *UBVRIJHK* passbands using the Hartfield polarimeter (described by Brindle et al. (1986), and Bailey & Hough (1982)) on the 3.9-m AAT at Siding Spring Observatory, and the 3.8-m UKIRT at Mauna Kea Observatory. As shown in Figure 9, our results deviate by 2-3 σ from the best fit $\lambda_{\text{max}} - K$ relation found by Whittet et al. (1992).

This deviation, which is statistically significant, cannot be explained by measurement errors, and calls for further investigation. For this reasons, we have looked in more de-

tail the case of Vela1 95, which is included in the Whittet et al. sample. For this object, Whittet et al. (1992) determined a $\lambda_{\text{max}}=5500\pm 200 \text{ \AA}$, $P_{\text{max}}=8.08\pm 0.07 \%$ and $K=1.10\pm 0.06$. From our data, we determined $\lambda_{\text{max}}=5864\pm 7 \text{ \AA}$, $P_{\text{max}}=8.295\pm 0.004 \%$ and $K=1.34\pm 0.01$.

In Figure 10 we compare the Whittet et al. (1992) measurements of Vela1 95 to our FORS2 measurements. The figure also includes the Serkowski law best fit to Whittet et al.’s data ($\lambda_{\text{max}}=5521\pm 111 \text{ \AA}$, $P_{\text{max}}=8.08\pm 0.07 \%$ and $K=1.10\pm 0.05$; which is consistent to the Serkowski fit parameters in Whittet et al. (1992)), compared to a fit to FORS2 data ($\lambda_{\text{max}}=5864\pm 7 \text{ \AA}$, $P_{\text{max}} = 8.295\pm 0.004 \%$ and $K=1.34\pm 0.01$), and Whittet et al. *BVRI* data points only ($\lambda_{\text{max}}=5606\pm 126 \text{ \AA}$, $P_{\text{max}}=8.11 \pm 0.08 \%$ and $K=1.25\pm 0.19$). While the FORS2 data perfectly match the *B* and *V* measurements by Whittet et al., a significant difference is seen in *R* and *I* passbands. This strongly suggests that the problem does not reside in the different wavelength ranges used in the two studies. The explanation for the observed discrepancy is most likely related to the effective wavelengths adopted by Whittet et al. (1992) in their work. The authors list the bandpass properties in their Table 1. They also remark that their *K* measurements are at an effective wavelength of $2.04 \mu\text{m}$ rather than at the usual value of $2.2\mu\text{m}$. This is justified by an absorption in the Foster prism, which narrows the passband and reduces the effective wavelength. However, the authors do not explain why they do not adopt the usual *R* and *I* values given in the instrument description (Brindle et al. (1986); Bailey & Hough (1982)). The central wavelengths reported by Whittet et al. (1992) are: $0.36 \mu\text{m}$ (*U*), $0.43 \mu\text{m}$ (*B*), $0.55 \mu\text{m}$ (*V*), $0.63 \mu\text{m}$ (*R*), $0.78 \mu\text{m}$ (*I*), $1.21 \mu\text{m}$ (*J*), $1.64 \mu\text{m}$ (*H*) and $2.04 \mu\text{m}$ (*K*). On the other hand, Brindle et al. (1986) list the following wavelengths: $0.36 \mu\text{m}$ (*U*), $0.43 \mu\text{m}$ (*B*), $0.55 \mu\text{m}$ (*V*), $0.72 \mu\text{m}$ (*R*), $0.80 \mu\text{m}$ (*I*), $1.2 \mu\text{m}$ (*J*), $1.64 \mu\text{m}$ (*H*) and $2.19 \mu\text{m}$ (*K*), which are also consistent with wavelengths in Bailey & Hough (1982), except that the latter specify $2.14 \mu\text{m}$ for the effective wavelength of the *K* passband. The difference in the *R* and *I* effective wavelengths is evident.

When using $0.72 \mu\text{m}$ and $0.80 \mu\text{m}$ for *R* and *I* respectively, a Serkowski law fit to all polarimetric points gives: $\lambda_{\text{max}}=5732\pm 160 \text{ \AA}$, $P_{\text{max}}=8.28\pm 0.12 \%$ and $K=1.24\pm 0.09$. When fitting the *BVRI* data only, the best fit parameters are: $\lambda_{\text{max}}=5834\pm 168 \text{ \AA}$, $P_{\text{max}}=8.42\pm 0.22 \%$ and $K=1.65\pm 0.45$. The results are summarized in Table 3. Since spectropolarimetric data do not suffer from the additional problem caused by the need of properly characterizing the photometric system, and given the superior quality of the data presented here and its higher signal to noise, we tend to believe our results are very robust and provide a solid reference. On these grounds, we suspect that the λ_{max} , P_{max} and K values reported by Whittet et al. (1992) are systematically smaller than real. We will further investigate this problem and its consequences in a separate study, using observations along the lines of sight to a larger sample of Galactic reddened stars.

5 SUMMARY AND CONCLUSIONS

In this study we used archival FORS2 observations of polarimetric standard stars to characterize the performance

² <http://www.eso.org/sci/facilities/paranal/instruments/fors/inst/pola.html>

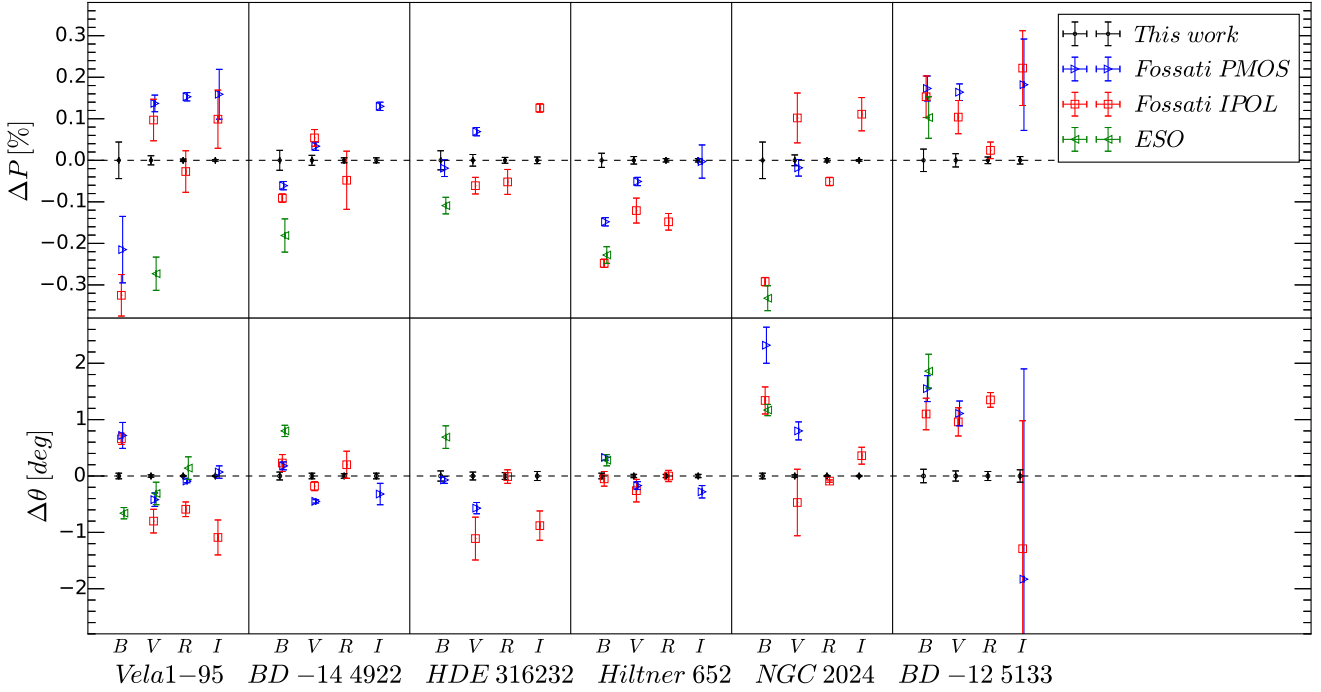


Figure 8. Comparison between IPOL and PMOS values presented in Fossati et al. (2007) (their Table 2), the ESO values given in the FORS webpage, and the new values obtained in this work. ΔP and $\Delta\theta$ are offsets from values obtained in this work. Three data points are outside of axis limits: the offset, ΔP , from the ESO value for Vela1 95, is $0.60 \pm 0.03\%$ and $-0.76 \pm 0.04\%$ in B and R band respectively, while ΔP in B band, from PMOS value (Fossati et al. 2007) for NGC 2024 1 is $\Delta P = -0.51 \pm 0.06\%$.

Table 3. Serkowski parameters comparison table.

	λ_{\max} (\AA)	P_{\max} (%)	K
Whittet et al. (1992)	5500 ± 200	8.08 ± 0.07	1.10 ± 0.06
Best fit to FORS2 data	5864 ± 7	8.295 ± 0.004	1.34 ± 0.01
Best fit to all Whittet et al. data points	5521 ± 111	8.08 ± 0.07	1.10 ± 0.05
Best fit to Whittet et al. $BVRI$ data only	5606 ± 126	8.11 ± 0.08	1.25 ± 0.19
Best fit to Whittet et al. $UBVR'I'JHK$ data	5732 ± 160	8.28 ± 0.12	1.24 ± 0.09
Best fit to Whittet et al. $BVR'I'$ data only	5834 ± 168	8.42 ± 0.22	1.65 ± 0.45

R' and I' indicate the modified passband wavelengths, $0.72 \mu\text{m}$ and $0.80 \mu\text{m}$ for R and I respectively.

and stability of FORS2 mounted at the VLT. For this purpose we analyzed 8 unpolarized standard stars observed on 40 epochs, and 6 polarized standard stars (30 epochs). Our main results can be summarized as follows:

(i) We confirm the instrumental wavelength dependent polarization detected by Fossati et al. (2007). The spurious signal steadily grows from the blue to the red, ranging from 0.05% (4000\AA) to 0.10% (9000\AA). The vectorial correction for P_Q and P_U (see Equation 7) can be applied to the observed Stokes parameters. The physical cause of this instrumental polarization is still unclear, but it is most likely related to the tilted surfaces of the dispersive element.

(ii) We tested the repeatability of total linear polarization using observations of polarized standard stars spanning 5 years. The RMS variation is $\lesssim 0.2\%$. For comparison, the typical error per 50\AA bin for a single epoch is $\lesssim 0.1\%$.

(iii) Using the same sample of polarized stars, we tested the HWP positioning stability, and found a RMS of 0.27° .

For comparison, the typical uncertainty in the weighted mean is $\sigma_\theta \lesssim 0.05^\circ$, while the typical uncertainty per 50\AA bin for a single epoch is $\lesssim 0.5^\circ$.

(iv) Our analysis confirms that FORS2 can achieve a maximum accuracy of $\sim 0.1\%$ and ~ 0.3 degrees in polarization degree and angle, respectively. These values, which represent the instrumental limits of this focal reducer, are shown to be stable over timescales of years.

(v) As a by-product of our analysis, we studied the wavelength dependence of linear polarization for our set of polarized standard stars. Our polarization results are in good agreement with those reported in the literature (see Figure 8). Peak polarization (P_{\max}), peak wavelength (λ_{\max}) and width parameter (K) were determined via least squares fit of the classical Serkowski law to the observed data.

(vi) Given the larger telescope size and the superb performance of FORS2, the data presented in this paper provide a robust re-calibration of a selected set of linear polarization standard stars that can be reliably used for both checking

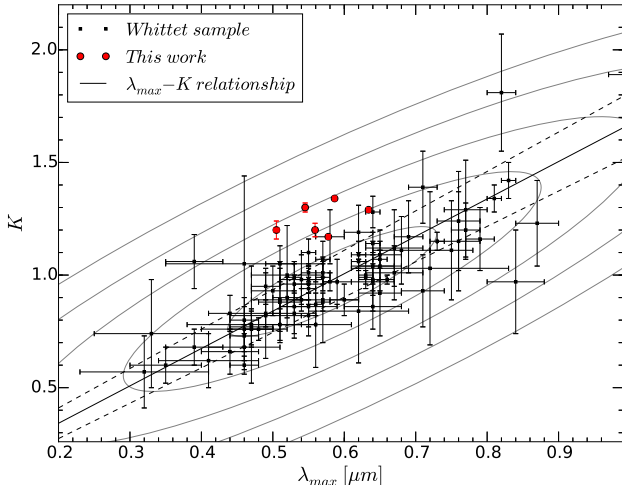


Figure 9. $\lambda_{\max} - K$ plane containing our 6 standard stars (red dots) compared to the sample from Whittet et al. (1992) (black dots). The full line is the empirical $\lambda_{\max} - K$ relationship determined in Whittet et al. (1992), and the dashed lines trace the 1σ uncertainty. The gray curves are 1 to 5 sigma error ellipses.

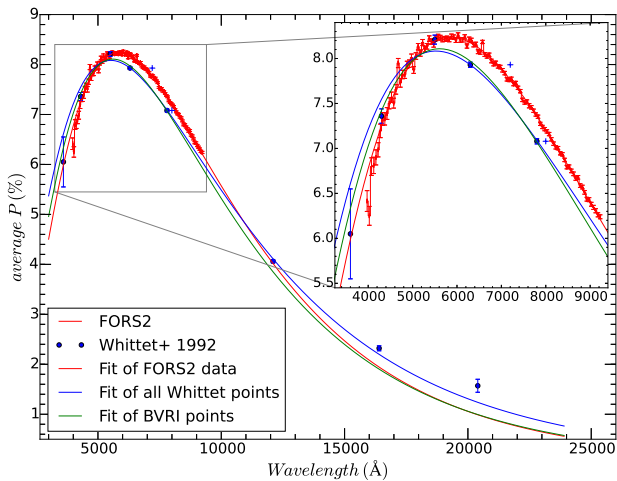


Figure 10. Comparison between Whittet et al. (1992) polarimetric measurements (blue dots) and spectropolarimetric FORS2 data (red line) for Vela1 95. The colored curves trace a best fit Serkowski law to all data points (blue), *BVRI* data points only (green) and FORS2 data (red). Blue '+' signs mark the effective wavelengths of *R* (0.72 μm) and *I* (0.80 μm) passbands, as specified in Brindle et al. (1986) and Bailey & Hough (1982).

the performance of other polarimeters and calibrating scientific data obtained with those instruments.

(vii) A comparison between the $\lambda_{\max} - K$ values presented in this paper and those reported by Whittet et al. (1992) reveals a systematic and statistically significant deviation, with our *K* values being larger. While this is partially caused by the shorter wavelength range covered by our FORS2 observations (4000-9000Å to be compared to the *UBVRIJHK* measurements by Whittet et al.), it is clear that this cannot fully explain the observed differences. A closer investigation shows that the *K* values reported by Whittet et al. (1992)

are most likely offset because of incorrect effective wavelengths for *R* and *I* passbands. This is clearly visible when comparing the data for the standard star Vela1 95, which is common to both data sets.

(viii) We expect that further studies, including larger sets of reddened Galactic stars, will show the same systematic discrepancy.

ACKNOWLEDGEMENTS

Based on observations made with ESO Telescopes at the Paranal Observatory under programme ID 60.A-9800, 60.A-9203, 084.B-0217, 084.D-0799, 085.D-0391, 089.D-0515, 091.D-0401, 290.D-5009.

REFERENCES

- Appenzeller I., 1967, *PASP*, **79**, 136
 Appenzeller I., et al., 1998, *The Messenger*, **94**, 1
 Bagnulo S., Landolfi M., Landstreet J. D., Landi Degl’Innocenti E., Fossati L., Sterzik M., 2009, *PASP*, **121**, 993
 Bailey J., Hough J. H., 1982, *PASP*, **94**, 618
 Brindle C., Hough J. H., Bailey J. A., Axon D. J., Hyland A. R., 1986, *MNRAS*, **221**, 739
 ESO 2015, FORS2 User Manual, issue 96.0, VLT-MAN-ESO-13100-1543. European Southern Observatory
 Fossati L., Bagnulo S., Mason E., Landi Degl’Innocenti E., 2007, in Sterken C., ed., *Astronomical Society of the Pacific Conference Series Vol. 364, The Future of Photometric, Spectrophotometric and Polarimetric Standardization*. p. 503
 Masiero J., Hodapp K., Harrington D., Lin H., 2007, *PASP*, **119**, 1126
 Patat F., Romaniello M., 2006, *PASP*, **118**, 146
 Patat F., Taubenberger S., 2011, *A&A*, **529**, A57
 Scarrott S. M., 1996, *QJRAS*, **37**, 297
 Scarrott S. M., Foley N. B., Gledhill T. M., Wolstencroft R. D., 1996, *MNRAS*, **282**, 252
 Serkowski K., Mathewson D. S., Ford V. L., 1975, *ApJ*, **196**, 261
 Wang L., Wheeler J. C., 2008, *ARA&A*, **46**, 433
 Whittet D. C. B., Martin P. G., Hough J. H., Rouse M. F., Bailey J. A., Axon D. J., 1992, *ApJ*, **386**, 562

Table 4: Unpolarized stars.

Name	Epoch	Passband	F_Q (%)	F_U (%)	S/N
HD10038	2010-09-24	all	0.076 ± 0.05	-0.025 ± 0.052	
		B	0.065 ± 0.012	-0.02 ± 0.013	1553
		V	0.065 ± 0.009	-0.025 ± 0.01	1927
		R	0.079 ± 0.005	-0.034 ± 0.006	1726
HD10038	2010-10-02	I	0.077 ± 0.007	-0.032 ± 0.008	1282
		all	0.027 ± 0.084	-0.002 ± 0.08	
		B	0.023 ± 0.022	0.027 ± 0.021	908
		V	0.012 ± 0.016	0.011 ± 0.015	1174
HD10038	2011-12-10	R	0.023 ± 0.009	0.008 ± 0.009	1062
		I	0.013 ± 0.012	-0.008 ± 0.011	799
		all	0.041 ± 0.061	-0.048 ± 0.062	
		B	0.031 ± 0.014	-0.055 ± 0.014	1317
HD10038	2012-12-25	V	0.035 ± 0.011	-0.053 ± 0.012	1608
		R	0.049 ± 0.007	-0.064 ± 0.007	1428
		I	0.045 ± 0.009	-0.042 ± 0.009	1050
		all	0.043 ± 0.086	0.021 ± 0.084	
HD10038	2013-12-14	B	0.045 ± 0.021	-0.0 ± 0.02	917
		V	0.046 ± 0.016	0.005 ± 0.016	1152
		R	0.051 ± 0.009	0.023 ± 0.009	1032
		I	0.044 ± 0.012	0.038 ± 0.012	768
HD10038	2015-07-31	all	0.052 ± 0.061	-0.031 ± 0.062	
		B	0.041 ± 0.014	-0.062 ± 0.014	1334
		V	0.046 ± 0.011	-0.033 ± 0.012	1608
		R	0.055 ± 0.007	-0.032 ± 0.007	1424
HD10038	2015-08-28	I	0.059 ± 0.009	-0.007 ± 0.009	1045
		all	0.04 ± 0.053	-0.029 ± 0.054	
		B	0.037 ± 0.014	-0.034 ± 0.014	1378
		V	0.032 ± 0.011	-0.023 ± 0.011	1760
HD10038	2015-10-14	R	0.041 ± 0.006	-0.028 ± 0.006	1600
		I	0.032 ± 0.008	-0.025 ± 0.008	1230
		all	0.078 ± 0.055	-0.063 ± 0.053	
		B	0.03 ± 0.013	-0.07 ± 0.013	1459
HD10038	2015-10-14	V	0.065 ± 0.01	-0.056 ± 0.01	1806
		R	0.083 ± 0.006	-0.06 ± 0.006	1621
		I	0.094 ± 0.008	-0.046 ± 0.008	1214
		all	0.041 ± 0.068	-0.117 ± 0.064	
HD13588	2014-10-02	B	-0.003 ± 0.017	-0.117 ± 0.016	1185
		V	0.053 ± 0.013	-0.09 ± 0.012	1478
		R	0.063 ± 0.007	-0.108 ± 0.007	1331
		I	0.054 ± 0.01	-0.146 ± 0.009	1002
HD13588	2015-08-14	all	0.11 ± 0.056	0.034 ± 0.055	
		B	0.154 ± 0.014	0.001 ± 0.014	1360
		V	0.101 ± 0.011	0.021 ± 0.011	1751
		R	0.106 ± 0.006	0.05 ± 0.006	1586
HD13588	2015-08-26	I	0.113 ± 0.008	0.048 ± 0.008	1196
		all	0.151 ± 0.075	-0.011 ± 0.078	
		B	0.099 ± 0.017	-0.058 ± 0.017	1054
		V	0.147 ± 0.014	0.002 ± 0.015	1273
HD13588	2015-10-14	R	0.15 ± 0.008	-0.02 ± 0.009	1127
		I	0.165 ± 0.011	-0.01 ± 0.011	831
		all	0.067 ± 0.068	0.047 ± 0.068	
		B	0.049 ± 0.015	0.027 ± 0.015	1635
HD13588	2015-10-14	V	0.057 ± 0.013	0.038 ± 0.013	1952
		R	0.067 ± 0.007	0.042 ± 0.007	1713
		I	0.074 ± 0.01	0.057 ± 0.01	1249
		all	0.149 ± 0.082	0.055 ± 0.087	
HD97689	2011-02-04	B	0.084 ± 0.018	0.029 ± 0.019	1303
		V	0.134 ± 0.016	0.04 ± 0.016	1573
		R	0.164 ± 0.009	0.048 ± 0.01	1389
		I	0.183 ± 0.012	0.081 ± 0.013	1023
HD97689	2011-02-12	all	0.063 ± 0.092	-0.028 ± 0.087	
		B	0.036 ± 0.021	-0.051 ± 0.02	912
		V	0.057 ± 0.017	-0.018 ± 0.016	1123
		R	0.07 ± 0.01	-0.006 ± 0.009	996
HD97689	2011-06-30	I	0.065 ± 0.013	-0.014 ± 0.013	733
		all	0.051 ± 0.057	0.017 ± 0.055	
		B	0.047 ± 0.012	-0.014 ± 0.012	1533
		V	0.038 ± 0.01	0.003 ± 0.01	1843
HD97689	2012-01-20	R	0.05 ± 0.006	0.007 ± 0.006	1613
		I	0.044 ± 0.008	0.048 ± 0.008	1154
		all	0.275 ± 0.056	0.042 ± 0.056	
		B	0.183 ± 0.013	0.014 ± 0.012	1470
HD97689	2012-03-30	V	0.235 ± 0.01	0.029 ± 0.01	1781
		R	0.266 ± 0.006	0.043 ± 0.006	1571
		I	0.333 ± 0.008	0.066 ± 0.008	1147
		all	0.159 ± 0.077	-0.012 ± 0.062	
HD97689	2013-05-06	B	0.113 ± 0.019	0.01 ± 0.015	1152
		V	0.144 ± 0.015	-0.006 ± 0.012	1442
		R	0.138 ± 0.008	-0.001 ± 0.007	1294
		I	0.173 ± 0.011	-0.039 ± 0.009	960
HD97689	2014-01-06	all	0.104 ± 0.062	0.051 ± 0.068	
		B	0.089 ± 0.014	0.019 ± 0.016	1232
		V	0.085 ± 0.012	0.025 ± 0.013	1522
		R	0.104 ± 0.007	0.047 ± 0.007	1356
HD97689	2014-12-24	I	0.122 ± 0.009	0.084 ± 0.01	999
		all	0.062 ± 0.055	-0.022 ± 0.053	
		B	0.071 ± 0.013	-0.008 ± 0.012	1482
		V	0.064 ± 0.01	-0.041 ± 0.01	1835
HD97689	2015-02-15	R	0.065 ± 0.006	-0.02 ± 0.006	1631
		I	0.063 ± 0.008	-0.039 ± 0.008	1201
		all	0.095 ± 0.059	0.026 ± 0.06	
		B	0.065 ± 0.014	-0.015 ± 0.014	1343
HD97689	2015-04-07	V	0.075 ± 0.011	0.011 ± 0.011	1661
		R	0.096 ± 0.006	0.026 ± 0.006	1483
		I	0.199 ± 0.008	0.058 ± 0.009	1094
		all	0.033 ± 0.08	-0.028 ± 0.081	
HD97689	2015-04-07	B	0.008 ± 0.018	-0.015 ± 0.018	1022
		V	0.018 ± 0.015	-0.018 ± 0.015	1229
		R	0.033 ± 0.009	-0.045 ± 0.009	1082
		I	0.036 ± 0.012	-0.035 ± 0.012	794
HD97689	2015-04-07	all	0.099 ± 0.059	0.035 ± 0.06	
		B	0.055 ± 0.013	0.017 ± 0.013	1387
		V	0.043 ± 0.011	0.025 ± 0.011	1705
		R	0.066 ± 0.006	0.03 ± 0.006	1501
HD97689	2015-04-07	I	0.143 ± 0.009	0.016 ± 0.009	1092
		all	-0.01 ± 0.057	0.053 ± 0.058	
		B	-0.012 ± 0.014	0.042 ± 0.014	1334
		V	-0.001 ± 0.011	0.054 ± 0.011	1691
HD97689	2015-04-07	R	-0.004 ± 0.006	0.048 ± 0.006	1523
		I	-0.024 ± 0.008	0.048 ± 0.008	1141

Table 4: continued.

Name	Epoch	Passband	P_Q (%)	P_U (%)	S/N
HD97689	2015-04-07	all	0.009 ± 0.084	-0.078 ± 0.092	
		<i>B</i>	-0.041 ± 0.023	-0.066 ± 0.025	829
		<i>V</i>	-0.018 ± 0.017	-0.018 ± 0.019	1073
		<i>R</i>	-0.006 ± 0.009	-0.058 ± 0.01	985
		<i>I</i>	0.053 ± 0.012	-0.122 ± 0.013	776
HD97689	2015-04-07	all	0.137 ± 0.077	0.089 ± 0.074	
		<i>B</i>	0.142 ± 0.021	0.002 ± 0.02	976
		<i>V</i>	0.103 ± 0.016	0.045 ± 0.015	1246
		<i>R</i>	0.135 ± 0.009	0.082 ± 0.008	1140
		<i>I</i>	0.136 ± 0.011	0.151 ± 0.01	894
HD42078	2010-04-07	all	0.024 ± 0.046	0.035 ± 0.045	
		<i>B</i>	0.066 ± 0.01	0.035 ± 0.01	1854
		<i>V</i>	0.041 ± 0.008	0.056 ± 0.008	2217
		<i>R</i>	0.046 ± 0.005	0.053 ± 0.005	1949
		<i>I</i>	-0.009 ± 0.007	0.011 ± 0.007	1419
HD42078	2010-10-14	all	0.161 ± 0.077	0.13 ± 0.072	
		<i>B</i>	0.132 ± 0.019	0.077 ± 0.018	1096
		<i>V</i>	0.143 ± 0.015	0.056 ± 0.014	1367
		<i>R</i>	0.162 ± 0.008	0.086 ± 0.008	1230
		<i>I</i>	0.191 ± 0.011	0.186 ± 0.01	924
HD42078	2010-12-13	all	0.053 ± 0.06	0.044 ± 0.061	
		<i>B</i>	0.051 ± 0.013	0.034 ± 0.014	1379
		<i>V</i>	0.046 ± 0.011	0.026 ± 0.011	1661
		<i>R</i>	0.055 ± 0.006	0.045 ± 0.007	1459
		<i>I</i>	0.061 ± 0.009	0.055 ± 0.009	1065
HD42078	2010-12-17	all	0.092 ± 0.069	-0.07 ± 0.072	
		<i>B</i>	0.089 ± 0.015	-0.077 ± 0.016	1183
		<i>V</i>	0.078 ± 0.013	-0.067 ± 0.013	1415
		<i>R</i>	0.101 ± 0.008	-0.08 ± 0.008	1246
		<i>I</i>	0.101 ± 0.01	-0.063 ± 0.011	911
HD42078	2014-03-04	all	0.173 ± 0.066	0.025 ± 0.065	
		<i>B</i>	0.158 ± 0.009	-0.059 ± 0.009	1604
		<i>V</i>	0.17 ± 0.01	-0.048 ± 0.009	1651
		<i>R</i>	0.204 ± 0.006	-0.013 ± 0.006	1348
		<i>I</i>	0.202 ± 0.011	0.087 ± 0.01	830
WD1615-154	2010-04-02	all	0.022 ± 0.083	0.023 ± 0.084	
		<i>B</i>	-0.007 ± 0.011	-0.006 ± 0.011	1440
		<i>V</i>	-0.028 ± 0.013	-0.003 ± 0.013	1388
		<i>R</i>	0.003 ± 0.009	0.029 ± 0.009	1088
		<i>I</i>	0.038 ± 0.013	0.014 ± 0.013	720
WD1620-391	2010-05-30	all	0.12 ± 0.168	-0.136 ± 0.168	
		<i>B</i>	0.014 ± 0.019	-0.059 ± 0.018	794
		<i>V</i>	0.124 ± 0.024	-0.01 ± 0.023	751
		<i>R</i>	0.115 ± 0.017	0.01 ± 0.017	547
		<i>I</i>	0.348 ± 0.028	-0.34 ± 0.028	339
WD1620-391	2010-07-14	all	0.062 ± 0.063	0.055 ± 0.065	
		<i>B</i>	0.042 ± 0.01	0.01 ± 0.01	1743
		<i>V</i>	0.038 ± 0.01	0.028 ± 0.011	1818
		<i>R</i>	0.06 ± 0.007	0.048 ± 0.007	1466
		<i>I</i>	0.078 ± 0.01	0.089 ± 0.01	992
WD1620-391	2011-02-11	all	0.056 ± 0.068	-0.011 ± 0.065	
		<i>B</i>	0.05 ± 0.01	-0.002 ± 0.01	1596
		<i>V</i>	0.053 ± 0.011	0.017 ± 0.01	1699
		<i>R</i>	0.068 ± 0.007	0.004 ± 0.007	1372
		<i>I</i>	0.057 ± 0.01	-0.049 ± 0.01	922
WD1620-391	2014-03-22	all	0.016 ± 0.062	0.026 ± 0.066	
		<i>B</i>	0.017 ± 0.009	0.004 ± 0.01	1746
		<i>V</i>	0.036 ± 0.01	-0.004 ± 0.011	1814
		<i>R</i>	0.047 ± 0.006	-0.01 ± 0.007	1447
		<i>I</i>	-0.023 ± 0.01	0.045 ± 0.01	968
WD1620-391	2014-03-22	all	0.009 ± 0.077	-0.004 ± 0.079	
		<i>B</i>	0.008 ± 0.011	-0.011 ± 0.012	1396
		<i>V</i>	-0.004 ± 0.012	0.015 ± 0.013	1452
		<i>R</i>	0.005 ± 0.008	0.016 ± 0.008	1160
		<i>I</i>	0.005 ± 0.012	-0.04 ± 0.012	778
WD1620-391	2014-03-22	all	-0.036 ± 0.078	-0.029 ± 0.078	
		<i>B</i>	-0.029 ± 0.011	-0.008 ± 0.011	1399
		<i>V</i>	-0.033 ± 0.013	-0.029 ± 0.013	1455
		<i>R</i>	-0.049 ± 0.008	-0.024 ± 0.008	1162
		<i>I</i>	-0.076 ± 0.012	-0.054 ± 0.012	778
WD1620-391	2015-02-26	all	0.018 ± 0.064	0.012 ± 0.065	
		<i>B</i>	-0.007 ± 0.009	-0.017 ± 0.009	1714
		<i>V</i>	-0.001 ± 0.01	-0.005 ± 0.01	1775
		<i>R</i>	0.006 ± 0.007	-0.009 ± 0.007	1415
		<i>I</i>	0.038 ± 0.01	0.029 ± 0.01	942
WD2039-202	2013-04-12	all	0.079 ± 0.073	0.038 ± 0.076	
		<i>B</i>	0.046 ± 0.012	-0.068 ± 0.013	1308
		<i>V</i>	0.072 ± 0.012	-0.009 ± 0.013	1464
		<i>R</i>	0.073 ± 0.008	0.014 ± 0.008	1199
		<i>I</i>	0.08 ± 0.011	0.05 ± 0.012	815
WD2039-202	2015-09-08	all	-0.011 ± 0.066	-0.039 ± 0.066	
		<i>B</i>	-0.003 ± 0.01	-0.038 ± 0.01	2143
		<i>V</i>	-0.008 ± 0.011	-0.056 ± 0.011	2275
		<i>R</i>	-0.006 ± 0.007	-0.041 ± 0.007	1831
		<i>I</i>	-0.02 ± 0.01	-0.039 ± 0.01	1234
WD2149+021	2011-10-11	all	-0.048 ± 0.056	-0.038 ± 0.056	
		<i>B</i>	-0.087 ± 0.009	-0.018 ± 0.009	1776
		<i>V</i>	-0.026 ± 0.009	-0.057 ± 0.009	2011
		<i>R</i>	-0.029 ± 0.006	-0.041 ± 0.006	1625
		<i>I</i>	-0.055 ± 0.009	-0.058 ± 0.009	1091

The signal-to-noise ratio, S/N, in individual bands is the average SNR between two 50Å bins, from 4250-4350Å (*B* band), 5450-5550Å (*V*), 6250-6350Å (*R*) and 7650-7850Å (*I*).

Table 5: Polarized stars.

Name	Epoch	Passband	P (%)	P_Q (%)	P_U (%)	θ (°)	S/N	Serkowski law		
								λ_{\max} (Å)	P_{\max} (%)	K
Velal-95	2010-04-07	<i>B</i>	7.69 ± 0.1	7.48 ± 0.1	-1.79 ± 0.1	172.72 ± 0.13	405	5848.2 ± 21.9	8.36 ± 0.01	1.34 ± 0.03
		<i>V</i>	8.23 ± 0.03	7.9 ± 0.03	-2.3 ± 0.03	172.43 ± 0.06	965			
		<i>R</i>	7.99 ± 0.01	7.61 ± 0.01	-2.42 ± 0.01	171.97 ± 0.04	1210			
		<i>I</i>	7.2 ± 0.01	6.95 ± 0.01	-1.91 ± 0.01	171.87 ± 0.03	1516			
Velal-95	2010-12-14	<i>B</i>	7.58 ± 0.12	7.39 ± 0.12	-1.68 ± 0.14	172.7 ± 0.15	328	5877.1 ± 22.8	8.27 ± 0.01	1.34 ± 0.03

Table 5: continued.

Name	Epoch	Passband	P (%)	P_Q (%)	P_U (%)	θ ($^\circ$)	S/N	Serkowski law		
								λ_{\max} (Å)	P_{\max} (%)	K
Vela1-95	2011-12-22	V	8.14 ± 0.03	7.8 ± 0.03	-2.32 ± 0.04	172.27 ± 0.07	801	5908.3 ± 25.1	8.25 ± 0.02	1.4 ± 0.04
		R	7.91 ± 0.01	7.54 ± 0.01	-2.41 ± 0.01	171.91 ± 0.04	1013			
		I	7.14 ± 0.01	6.88 ± 0.01	-1.89 ± 0.01	171.87 ± 0.04	1287			
		B	7.58 ± 0.14	7.37 ± 0.14	-1.78 ± 0.14	172.53 ± 0.18	304			
Vela1-95	2013-12-03	V	8.08 ± 0.04	7.75 ± 0.04	-2.3 ± 0.04	172.3 ± 0.08	739	5913.5 ± 17.4	8.29 ± 0.01	1.38 ± 0.02
		R	7.91 ± 0.01	7.55 ± 0.01	-2.38 ± 0.01	172.06 ± 0.05	930			
		I	7.11 ± 0.01	6.85 ± 0.01	-1.91 ± 0.01	171.76 ± 0.05	1175			
		B	7.59 ± 0.15	7.41 ± 0.15	-1.65 ± 0.17	173.13 ± 0.18	378			
Vela1-95	2013-12-05	V	8.13 ± 0.04	7.83 ± 0.04	-2.2 ± 0.04	172.78 ± 0.08	911	5869.6 ± 23.3	8.31 ± 0.01	1.36 ± 0.03
		R	7.94 ± 0.01	7.59 ± 0.01	-2.32 ± 0.01	172.32 ± 0.05	1157			
		I	7.17 ± 0.01	6.93 ± 0.01	-1.85 ± 0.01	172.1 ± 0.05	1486			
		B	7.63 ± 0.14	7.43 ± 0.14	-1.72 ± 0.17	172.83 ± 0.17	301			
Vela1-95	2013-12-31	V	8.17 ± 0.04	7.85 ± 0.04	-2.27 ± 0.04	172.56 ± 0.08	740	5848.3 ± 21.6	8.28 ± 0.01	1.34 ± 0.03
		R	7.93 ± 0.01	7.58 ± 0.01	-2.35 ± 0.01	172.19 ± 0.05	951			
		I	7.17 ± 0.01	6.92 ± 0.01	-1.85 ± 0.01	172.1 ± 0.04	1240			
		B	7.68 ± 0.15	7.51 ± 0.15	-1.61 ± 0.15	173.19 ± 0.18	290			
Vela1-95	2014-01-06	V	8.15 ± 0.04	7.86 ± 0.04	-2.16 ± 0.04	172.89 ± 0.08	695	5881.1 ± 19.3	8.32 ± 0.01	1.35 ± 0.03
		R	7.91 ± 0.01	7.58 ± 0.01	-2.28 ± 0.01	172.42 ± 0.05	880			
		I	7.14 ± 0.01	6.91 ± 0.01	-1.81 ± 0.01	172.22 ± 0.05	1127			
		B	7.63 ± 0.12	7.45 ± 0.12	-1.67 ± 0.13	172.86 ± 0.14	352			
Vela1-95	2014-12-22	V	8.19 ± 0.03	7.88 ± 0.03	-2.25 ± 0.03	172.59 ± 0.06	874	5831.1 ± 31.7	8.26 ± 0.02	1.34 ± 0.04
		R	7.95 ± 0.01	7.61 ± 0.01	-2.32 ± 0.01	172.35 ± 0.04	1123			
		I	7.19 ± 0.01	6.95 ± 0.01	-1.85 ± 0.01	172.11 ± 0.04	1467			
		B	7.57 ± 0.18	7.36 ± 0.18	-1.78 ± 0.18	172.5 ± 0.21	244			
Vela1-95	2015-01-17	V	8.18 ± 0.05	7.82 ± 0.05	-2.39 ± 0.05	171.97 ± 0.1	585	5695.0 ± 83.7	8.23 ± 0.04	1.21 ± 0.09
		R	7.87 ± 0.01	7.49 ± 0.01	-2.43 ± 0.01	171.77 ± 0.06	742			
		I	7.12 ± 0.01	6.86 ± 0.01	-1.89 ± 0.01	171.87 ± 0.05	960			
		B	7.72 ± 0.24	7.51 ± 0.24	-1.77 ± 0.26	172.63 ± 0.28	171			
Vela1-95	2015-05-30	V	8.11 ± 0.06	7.76 ± 0.06	-2.37 ± 0.07	172.02 ± 0.13	415	5866.9 ± 40.9	8.18 ± 0.02	1.3 ± 0.05
		R	7.81 ± 0.02	7.43 ± 0.02	-2.42 ± 0.02	171.8 ± 0.08	526			
		I	7.03 ± 0.01	6.76 ± 0.01	-1.91 ± 0.01	171.69 ± 0.08	678			
		B	7.52 ± 0.25	7.16 ± 0.25	-2.3 ± 0.25	170.57 ± 0.31	168			
Vela1-95	2015-12-29	V	8.05 ± 0.06	7.64 ± 0.06	-2.53 ± 0.06	171.38 ± 0.14	422	5692.1 ± 30.6	8.34 ± 0.02	1.22 ± 0.03
		R	7.84 ± 0.02	7.41 ± 0.02	-2.57 ± 0.02	171.21 ± 0.08	539			
		I	7.09 ± 0.01	6.8 ± 0.01	-2.02 ± 0.01	171.3 ± 0.08	695			
		B	7.9 ± 0.18	7.72 ± 0.18	-1.69 ± 0.18	173.17 ± 0.2	260			
BD-144922	2011-10-02	V	8.21 ± 0.04	7.86 ± 0.04	-2.37 ± 0.04	172.23 ± 0.09	673	5429.6 ± 21.0	6.14 ± 0.01	1.33 ± 0.03
		R	7.91 ± 0.01	7.52 ± 0.01	-2.45 ± 0.01	171.82 ± 0.05	879			
		I	7.11 ± 0.01	6.86 ± 0.01	-1.89 ± 0.01	171.86 ± 0.05	1184			
		B	7.9 ± 0.18	7.72 ± 0.18	-1.69 ± 0.18	173.17 ± 0.2	260			
BD-144922	2013-03-06	V	5.82 ± 0.04	-1.06 ± 0.04	5.72 ± 0.04	50.01 ± 0.11	667	5470.4 ± 18.6	6.14 ± 0.01	1.32 ± 0.03
		R	6.09 ± 0.02	-0.99 ± 0.02	6.01 ± 0.02	50.0 ± 0.07	1133			
		I	5.8 ± 0.01	-0.88 ± 0.01	5.73 ± 0.01	49.85 ± 0.06	1180			
		B	4.96 ± 0.01	-0.8 ± 0.01	4.89 ± 0.01	49.29 ± 0.07	1096			
HDE316232	2010-07-14	V	5.79 ± 0.03	-0.95 ± 0.03	5.71 ± 0.03	49.5 ± 0.09	812	5591.1 ± 18.3	5.02 ± 0.01	1.22 ± 0.03
		R	6.1 ± 0.02	-0.93 ± 0.02	6.03 ± 0.02	49.66 ± 0.06	1296			
		I	5.83 ± 0.01	-0.85 ± 0.01	5.77 ± 0.01	49.58 ± 0.05	1302			
		B	5.02 ± 0.01	-0.79 ± 0.01	4.96 ± 0.01	49.18 ± 0.07	1126			
Hiltner652	2010-07-20	V	4.68 ± 0.02	4.64 ± 0.02	0.62 ± 0.02	3.61 ± 0.09	1063	5770.2 ± 18.3	6.46 ± 0.01	1.2 ± 0.03
		R	4.93 ± 0.01	4.9 ± 0.01	0.55 ± 0.01	3.51 ± 0.07	1529			
		I	4.77 ± 0.01	4.75 ± 0.01	0.51 ± 0.01	3.37 ± 0.06	1499			
		B	4.21 ± 0.01	4.18 ± 0.01	0.56 ± 0.01	3.53 ± 0.08	1272			
Hiltner652	2011-07-20	V	5.94 ± 0.04	5.94 ± 0.04	-0.08 ± 0.04	179.32 ± 0.11	691	5807.4 ± 31.3	6.48 ± 0.02	1.24 ± 0.05
		R	6.37 ± 0.02	6.37 ± 0.02	-0.21 ± 0.02	179.39 ± 0.07	1083			
		I	6.21 ± 0.01	6.21 ± 0.01	-0.23 ± 0.01	179.3 ± 0.06	1106			
		B	5.6 ± 0.01	5.6 ± 0.01	-0.05 ± 0.01	179.43 ± 0.07	978			
Hiltner652	2011-07-22	V	5.95 ± 0.06	5.95 ± 0.06	0.03 ± 0.05	179.85 ± 0.16	477	5816.4 ± 26.7	6.51 ± 0.01	1.15 ± 0.04
		R	6.36 ± 0.03	6.36 ± 0.03	-0.09 ± 0.03	179.94 ± 0.1	772			
		I	6.24 ± 0.01	6.24 ± 0.01	-0.12 ± 0.01	179.81 ± 0.08	797			
		B	5.62 ± 0.01	5.62 ± 0.01	0.05 ± 0.01	179.93 ± 0.1	714			
Hiltner652	2015-02-26	V	5.97 ± 0.05	5.97 ± 0.05	0.04 ± 0.05	0.09 ± 0.13	529	5788.8 ± 30.8	6.49 ± 0.02	1.16 ± 0.05
		R	6.42 ± 0.02	6.42 ± 0.02	-0.13 ± 0.02	179.69 ± 0.09	831			
		I	6.29 ± 0.01	6.29 ± 0.01	-0.13 ± 0.01	179.84 ± 0.07	839			
		B	5.71 ± 0.01	5.71 ± 0.01	0.08 ± 0.01	0.07 ± 0.09	723			
Hiltner652	2015-04-12	V	5.96 ± 0.06	5.96 ± 0.06	0.02 ± 0.06	179.94 ± 0.16	436	5795.0 ± 23.8	6.46 ± 0.01	1.15 ± 0.04
		R	6.41 ± 0.03	6.41 ± 0.03	-0.17 ± 0.03	179.55 ± 0.1	715			
		I	6.24 ± 0.01	6.23 ± 0.01	-0.2 ± 0.01	179.49 ± 0.08	740			
		B	5.65 ± 0.01	5.65 ± 0.01	-0.05 ± 0.01	179.41 ± 0.1	675			
Hiltner652	2015-04-12	V	5.95 ± 0.05	5.95 ± 0.05	-0.11 ± 0.05	179.18 ± 0.14	516	5759.0 ± 24.8	6.51 ± 0.01	1.16 ± 0.04
		R	6.36 ± 0.02	6.36 ± 0.02	-0.23 ± 0.02	179.29 ± 0.09	865			
		I	6.22 ± 0.01	6.21 ± 0.01	-0.26 ± 0.01	179.21 ± 0.07	900			
		B	5.66 ± 0.01	5.66 ± 0.01	-0.06 ± 0.01	179.31 ± 0.09	794			
Hiltner652	2015-04-12	V	6.01 ± 0.06	6.0 ± 0.06	-0.09 ± 0.06	179.39 ± 0.17	569	5763.9 ± 32.9	6.4 ± 0.02	1.2 ± 0.05
		R	6.41 ± 0.03	6.41 ± 0.03	-0.24 ± 0.03	179.26 ± 0.11	939			
		I	6.26 ± 0.01	6.26 ± 0.01	-0.22 ± 0.01	179.38 ± 0.09	968			
		B	5.66 ± 0.01	5.66 ± 0.01	-0.06 ± 0.01	179.37 ± 0.11	843			
Hiltner652	2015-05-09	V	5.88 ± 0.05	5.88 ± 0.05	-0.07 ± 0.05	179.46 ± 0.15	479	5726.7 ± 25.8	6.42 ± 0.01	1.16 ± 0.04
		R	6.31 ± 0.03	6.31 ± 0.03	-0.24 ± 0.03	179.23 ± 0.1	756			
		I	6.15 ± 0.01	6.15 ± 0.01	-0.26 ± 0.01	179.21 ± 0.08	773			
		B	5.52 ± 0.01	5.52 ± 0.01	-0.11 ± 0.01	179.07 ± 0.1	709			
Hiltner652	2015-06-10	V	5.94 ± 0.04	5.94 ± 0.04	-0.11 ± 0.04	179.26 ± 0.12	600	6355.6 ± 10.1	9.87 ± 0.01	1.31 ± 0.02
		R	6.34 ± 0.02	6.33 ± 0.02	-0.25 ± 0.02	179.25 ± 0.08	933			
		I	6.17 ± 0.01	6.16 ± 0.01	-0.27 ± 0.01	179.05 ± 0.07	949			
		B	5.53 ± 0.01	5.53 ± 0.01	-0.1 ± 0.01	179.14 ± 0.08	831			
NGC2024	2010-12-31	V	9.55 ± 0.03	0.25 ± 0.03	-9.54 ± 0.03	136.33 ± 0.05	1008	6337.7 ± 11.7	9.78 ± 0.01	1.26 ± 0.02
		R	9.67 ± 0.01	0.09 ± 0.01	-9.67 ± 0.01	136.19 ± 0.03	1314			
		I	9.02 ± 0.0	0.49 ± 0.0	-9.0 ± 0.0	136.18 ± 0.02	1832			
		B	8.53 ± 0.1	0.74 ± 0.1	-8.5 ± 0.1	136.8 ± 0.1	449			
NGC2024	2011-12-30	V	9.55 ± 0.03	0.25 ± 0.03	-9.54 ± 0.03	136.33 ± 0.05	1008	6337.7 ± 11.7	9.78 ± 0.01	1.26 ± 0.02
		R	9.67 ± 0.01	0.09 ± 0.01	-9.67 ± 0.01	136.19 ± 0.03	1314			
		I	9.02 ± 0.0	0.49 ± 0.0	-9.0 ± 0.0	136.18 ± 0.02	1832			
		B	8.53 ± 0.1	0.74 ± 0.1	-8.5 ± 0.1	136.8 ± 0.1	449			

Table 5: continued.

Name	Epoch	Passband	P (%)	P_Q (%)	P_U (%)	θ ($^\circ$)	S/N	Serkowski law		
								λ_{\max} (Å)	P_{\max} (%)	K
NGC2024	2012-11-14	<i>B</i>	8.56 ± 0.12	0.63 ± 0.11	-8.54 ± 0.12	136.62 ± 0.12	408	6308.6 ± 12.4	9.95 ± 0.01	1.26 ± 0.02
		<i>V</i>	9.46 ± 0.03	0.13 ± 0.03	-9.46 ± 0.03	136.0 ± 0.05	927			
		<i>R</i>	9.59 ± 0.01	-0.02 ± 0.01	-9.59 ± 0.01	135.91 ± 0.03	1214			
		<i>I</i>	8.95 ± 0.01	0.34 ± 0.0	-8.95 ± 0.01	135.73 ± 0.02	1692			
NGC2024	2015-05-11	<i>B</i>	8.7 ± 0.12	0.74 ± 0.11	-8.67 ± 0.12	137.0 ± 0.11	408	6366.5 ± 13.0	10.0 ± 0.01	1.27 ± 0.02
		<i>V</i>	9.64 ± 0.03	0.27 ± 0.03	-9.63 ± 0.03	136.39 ± 0.05	911			
		<i>R</i>	9.75 ± 0.01	0.18 ± 0.01	-9.75 ± 0.01	136.47 ± 0.03	1193			
		<i>I</i>	9.08 ± 0.01	0.56 ± 0.01	-9.06 ± 0.01	136.4 ± 0.02	1662			
NGC2024	2015-09-25	<i>B</i>	8.69 ± 0.09	0.37 ± 0.11	-8.68 ± 0.09	135.74 ± 0.12	364	6310.4 ± 12.9	9.81 ± 0.01	1.27 ± 0.02
		<i>V</i>	9.64 ± 0.03	-0.04 ± 0.04	-9.64 ± 0.03	135.31 ± 0.06	735			
		<i>R</i>	9.86 ± 0.01	-0.11 ± 0.01	-9.85 ± 0.01	135.48 ± 0.04	845			
		<i>I</i>	9.19 ± 0.01	0.3 ± 0.01	-9.18 ± 0.01	135.59 ± 0.04	1016			
NGC2024	2015-10-14	<i>B</i>	8.57 ± 0.11	0.52 ± 0.11	-8.55 ± 0.11	136.22 ± 0.11	427	6363.9 ± 14.9	9.81 ± 0.01	1.3 ± 0.02
		<i>V</i>	9.51 ± 0.03	0.04 ± 0.03	-9.51 ± 0.03	135.68 ± 0.05	944			
		<i>R</i>	9.62 ± 0.01	-0.1 ± 0.01	-9.62 ± 0.01	135.64 ± 0.03	1230			
		<i>I</i>	8.95 ± 0.0	0.3 ± 0.01	-8.94 ± 0.0	135.58 ± 0.02	1703			
NGC2024	2015-10-14	<i>B</i>	8.47 ± 0.15	0.41 ± 0.16	-8.46 ± 0.15	135.91 ± 0.15	306	6339.6 ± 13.7	9.81 ± 0.01	1.25 ± 0.02
		<i>V</i>	9.49 ± 0.04	-0.0 ± 0.04	-9.49 ± 0.04	135.61 ± 0.07	701			
		<i>R</i>	9.62 ± 0.01	-0.14 ± 0.01	-9.62 ± 0.01	135.53 ± 0.04	927			
		<i>I</i>	8.99 ± 0.01	0.31 ± 0.01	-8.98 ± 0.01	135.6 ± 0.03	1327			
BD-125133	2015-09-08	<i>B</i>	8.58 ± 0.21	0.57 ± 0.21	-8.56 ± 0.21	136.29 ± 0.2	309	5049.5 ± 35.5	4.37 ± 0.01	1.17 ± 0.04
		<i>V</i>	9.5 ± 0.06	0.05 ± 0.06	-9.5 ± 0.06	135.73 ± 0.09	710			
		<i>R</i>	9.62 ± 0.01	-0.09 ± 0.01	-9.62 ± 0.01	135.7 ± 0.05	943			
		<i>I</i>	8.98 ± 0.01	0.37 ± 0.01	-8.97 ± 0.01	135.82 ± 0.04	1358			
		<i>B</i>	4.22 ± 0.03	1.69 ± 0.03	-3.86 ± 0.03	146.54 ± 0.12	845			
		<i>V</i>	4.27 ± 0.02	1.57 ± 0.02	-3.97 ± 0.02	145.88 ± 0.09	1252			
		<i>R</i>	4.0 ± 0.01	1.41 ± 0.01	-3.74 ± 0.01	145.62 ± 0.08	1213			
		<i>I</i>	3.35 ± 0.01	1.22 ± 0.01	-3.12 ± 0.01	145.28 ± 0.11	1049			

The polarization angle, θ , in individual bands is the average polarization angle from 3980-4920Å (*B* band), 5070-5950Å (*V*), 5890-5890Å (*R*) and 7310-8810Å (*I*). The signal-to-noise ratio, S/N, in individual bands is the average SNR between two 50Å bins, from 4250-4350Å (*B*), 5450-5550Å (*V*), 6250-6350Å (*R*) and 7650-7850Å (*I*).

This paper has been typeset from a $\text{\TeX}/\text{\LaTeX}$ file prepared by the author.

